

Let's keep brainstorming title ideas. I don't think our results support the idea of 'episodes of rapid expansion'

Trevor Drees^{*a,b}, Brad M. Ochocki^b, Scott L. Collins^c, and Tom E.X. Miller^b

^aDepartment of Biology, Penn State University, State College, PA USA

^bProgram in Ecology and Evolutionary Biology, Department of BioSciences, Rice University, Houston, TX USA

^cDepartment of Biology, University of New Mexico, Albuquerque, NM USA

July 22, 2021

^{*}thd5066@psu.edu

1 Abstract

2 **Encroachment**¹ of shrubs into adjacent grasslands has become an increasingly reported
3 phenomenon across the world, and such encroachment is either pulled forward by high
4 population growth at the low-density encroachment front or pushed forward by higher-
5 density areas behind the front. However, at sites such as Sevilleta National Wildlife
6 Refuge in central New Mexico, little is known about whether encroachment is pushed or
7 pulled, and the dynamics of encroachment are not well-understood. Here, long-term en-
8 croachment of creosotebush (*Larrea tridentata*), a native perennial shrub, stands in stark
9 contrast with the stagnation in encroachment observed in recent decades. In order to
10 better understand creosotebush encroachment at this site, we quantify it using a spatially
11 structured population model where a wave of individuals travels at a speed governed by
12 both dispersal and density-dependence. Results indicate that population growth rates
13 generally increase with decreasing density, suggesting that encroachment is pulled by
14 individuals at the low-density wave front, and the spatial population model predicts an
15 encroachment rate of less than 2 cm per year. While the predicted rate of encroach-
16 ment is consistent with observations over recent decades, it does not explain long-term
17 creosotebush encroachment at the study site, suggesting that this process may occur in
18 pulses when recruitment, seedling survival, or dispersal significantly exceed typical rates.
19 Overall, our work demonstrates that individuals at low densities are likely the biggest
20 contributors to creosotebush encroachment at this site, and that this encroachment is
21 likely a process that occurs in large but infrequent bursts rather than at a steady pace.

22 Keywords

23 density-dependence, ecotones, woody encroachment, shrubs, integral projection model,
24 grassland

¹*I am not editing the abstract for now.*

25 Introduction

26 The recent and ongoing encroachment of shrubs and other woody plants into adjacent
27 grasslands has caused significant vegetation changes across arid and semi-arid landscapes
28 worldwide (Van Auken, 2000, 2009; Goslee et al., 2003; Gibbens et al., 2005; Parizek et al.,
29 2002; Cabral et al., 2003; Trollope et al., 1989; Roques et al., 2001). The process of en-
30 croachment generally involves increases in the number or density of woody plants in both
31 time and space (Van Auken, 2000), which can drive shifts in plant community structure
32 and alter ecosystem processes (Schlesinger et al., 1990; Ravi et al., 2009; Schlesinger
33 and Pilmanis, 1998; Knapp et al., 2008). Other effects of encroachment include changes
34 in ecosystem services (Reed et al., 2015; Kelleway et al., 2017), declines in biodiversity
35 (Ratajczak et al., 2012; Sirami and Monadjem, 2012; Brandt et al., 2013), and economic
36 losses in areas where the proliferation of shrubs adversely affects grazing land and pastoral
37 production (Mugasi et al., 2000; Oba et al., 2000).

38 Woody plant encroachment can be studied through the lens of spatial population
39 biology as a wave of individuals that may expand across space and over time (Kot et al.,
40 1996; Neubert and Caswell, 2000; Wang et al., 2002; Pan and Lin, 2012). Theory pre-
41 dicts that the speed of wave expansion depends on two processes: local demography and
42 dispersal of propagules. First, local demographic processes include recruitment, survival,
43 growth, and reproduction, which collectively determine the rate at which newly colonized
44 locations increase in density and produce new propagules. Second, colonization events
45 are driven by the spatial dispersal of propagules, which is commonly summarized as a
46 probability distribution of dispersal distance, or “dispersal kernel”. The speed at which
47 expansion waves move is highly dependent upon the shape of the dispersal kernel, espe-
48 cially long-distance dispersal events in the tail of the distribution (Skarpaas and Shea,
49 2007). Both demography and dispersal may depend on plant size, since larger plants
50 often have improved demographic performance and release seeds from greater heights,

51 leading to longer dispersal distances (Nathan et al., 2011). Accounting for population
52 structure, including size structure, may therefore be important for understanding and
53 predicting wave expansion dynamics (Neubert and Caswell, 2000).

54 Theory predicts that the nature of conspecific density dependence is another critical
55 feature of expansion dynamics but this is rarely studied in the context of woody plant
56 encroachment. Expansion waves typically correspond to gradients of conspecific density
57 – high in the back and low at the front – and demographic rates may be sensitive to
58 density due to intraspecific interactions like competition or facilitation. If the demo-
59 graphic effects of density are strictly negative due to competitive effects that increase
60 with density then demographic performance is maximized as density goes to zero, at the
61 leading edge of the wave. Under these conditions, the wave is “pulled” forward by indi-
62 viduals at the low-density vanguard (Kot et al., 1996), and targeting these individuals
63 and locations would be the most effective way to slow down or prevent encroachment
64 (cite?). However, woody encroachment systems often involve positive feedbacks whereby
65 shrub establishment modifies the environment in ways that facilitate further shrub re-
66 cruitment. For example, woody plants can modify their micro-climates in ways that
67 elevate nighttime minimum temperatures, promoting conspecific recruitment and sur-
68 vival for freeze-sensitive species (D’Odorico et al., 2010; Huang et al., 2020). Such Allee
69 effects (in the language of population biology) cause demographic rates to be maximized
70 at higher densities behind the leading edge, which “push” the expansion forward, leading
71 to qualitatively different dynamics (Kot et al., 1996; Taylor and Hastings, 2005; Sullivan
72 et al., 2017; Lewis and Kareiva, 1993; Veit and Lewis, 1996; Keitt et al., 2001). Pushed
73 expansion waves generally have different shapes (steeper density gradients) and slower
74 speeds than pulled waves (Gandhi et al., 2016), and may require different strategies for
75 managing or decelerating expansion (check Taylor and Hastings ref). The potential for
76 positive feedbacks is well documented in woody encroachment systems but it remains
77 unclear whether and how strongly these feedbacks decelerate shrub expansion and influ-

78 ence strategies for management of woody encroachment. Despite decades of work on this
79 topic, we still do not know whether expansion waves of woody encroachment are pushed
80 or pulled.

81 In this study, we linked woody plant encroachment to ecological theory for invasion
82 waves, with the goals of understanding how seed dispersal and density-dependent demog-
83 raphy drive encroachment, and determining whether the encroachment wave is pushed or
84 pulled. Throughout the aridlands of the southwestern United States, shrub encroachment
85 into grasslands is well documented (cite) but little is known about the dispersal and de-
86 mographic processes that govern it. Our work focused on encroachment of creosotebush
87 (*Larrea tridentata*) in the northern Chihuahuan Desert. Expansion of this species into
88 grasslands over the past 150 years has been well documented, leading to decreased cover
89 of *Bouteloua eriopoda*, the dominant foundation species of Chihuahuan desert grassland
90 (Gardner, 1951; Buffington and Herbel, 1965; Gibbens et al., 2005). As in many woody
91 encroachment systems, creosotebush expansion generates ecotones marking a transition
92 from dense shrubland to open grassland, with a transition zone in between where shrubs
93 can often be found interspersed among grasses (Fig. 1).

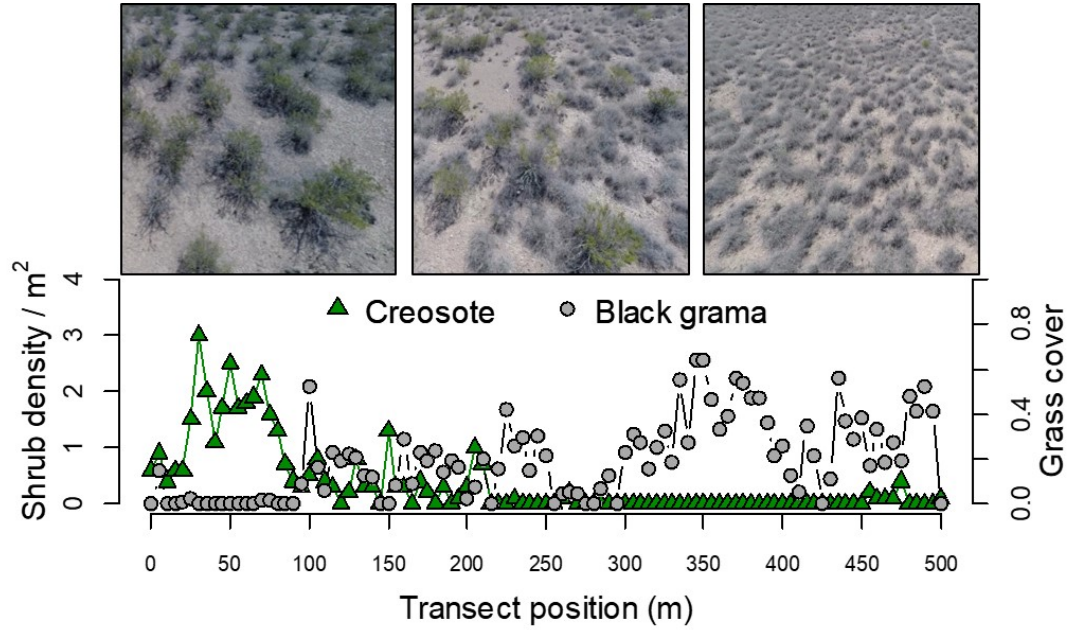


Figure 1: Caption.

Historically, creosotebush encroachment into grasslands is believed to have been driven by a combination of factors including overgrazing, drought, variability in rainfall, and suppression of fire regimes Moreno-de las Heras et al. (2016). These shrubs are also thought to further facilitate their own encroachment through positive feedbacks (Grover and Musick, 1990; D’Odorico et al., 2012) by modifying their environment in ways that favor continued growth and recruitment, such as the local micro-climate (D’Odorico et al., 2010) and rates of soil erosion (Turnbull et al., 2010). Such positive feedback also involve suppression of herbaceous competitors, reducing competition as well as the amount of flammable biomass used to fuel the fires that keep creosotebush growth in check (Van Auken, 2000). We hypothesized that, given potential for positive feedback mechanisms, the rarity of conspecifics at the low-density encroachment front may depress demographic performance and generate pushed-wave dynamics.

We used a combination of observational and experimental data from shrub ecotones

107 in central New Mexico to parameterize a spatial integral projection model (SIPM) that
 108 predicts that speed of encroachment (m/yr) resulting from lower-level demographic and
 109 dispersal processes. Our data came from demographic surveys and experimental trans-
 110 plants along replicate ecotone transects spanning a gradient of shrub density and seed
 111 drop experiments to infer the properties of the dispersal kernel. We focused on wind
 112 dispersal of seeds as a starting point, since little is known about the natural history
 113 of dispersal in this system and the seeds lack rewards to attract animal dispersers. We
 114 also used re-surveys of permanent transects as an independent measure of encroachment
 115 that provided a benchmark against which to evaluate model predictions. The SIPM ac-
 116 counts for size-structured demography of creosotebush, allows us to test whether shrub
 117 expansion is pulled by the low-density front or pushed from the high-density core, and
 118 identifies the local (demographic) and spatial (seed dispersal) life cycle transitions that
 119 most strongly contribute to expansion speed². We address the following specific ques-
 120 tions:

- 121 1. What is the observed rate of creosotebush encroachment in recent past?
- 122 2. How do creosotebush size and conspecific density affect variation in demographic
 123 vital rates (survival, growth, reproduction, and recruitment) along shrub encroach-
 124 ment ecotones?
- 125 3. What is the wind dispersal kernel for this species and how far do seeds typically
 126 travel by wind?
- 127 4. What is the predicted rate of expansion from the SIPM and what lower-level pro-
 128 cesses most strongly govern the expansion speed?
- 129 5. Is encroachment pulled by the individuals at the front of the wave or pushed by
 130 individuals behind it?

²*we will need to stay consistent with the language of encroachment/expansion/invasion. For now I am swictihg a lot.*

131 **Materials and methods**

132 **Study species**

133 Creosotebush *Larrea tridentata* is a perennial, drought-resistant shrub that is native to
134 the arid and semiarid regions of the southwestern United States and northern Mexico.
135 High-density areas of creosotebush consist largely of barren soil between plants due to
136 the “islands of fertility” these shrubs create around themselves (Schlesinger et al., 1996;
137 Reynolds et al., 1999), though lower-density areas will often contain grasses in the in-
138 tershrub spaces (Fig. 1). In our northern Chihuahuan desert study region creosotebush
139 reproduces sexually, with numerous small yellow flowers giving rise to highly pubescent
140 spherical fruits several millimetres in diameter; these fruits consist of five carpels, each
141 of which contains a single seed. Seeds are dispersed from the parent plant by gravity
142 and wind, with the possibility for seeds to also be blown across the soil surface or trans-
143 ported by water runoff (Maddox and Carlquist, 1985). In other regions, this species also
144 reproduces asexually and can give rise to long-lived clonal stands (Vasek, 1980), but this
145 does not occur in our study region. The foliage is dark green, resinous, and unpalatable
146 to most grazing and browsing animals (Mabry et al., 1978).

147 **Study site**

148 We conducted our experiments and censuses at the Sevilleta National Wildlife Refuge
149 (SNWR), a Long-Term Ecological Research (LTER) site in central New Mexico. The
150 refuge exists at the intersection of several eco-regions, including the Chihuahuan Desert
151 and steppes of the Colorado Plateau. Annual precipitation is low at approximately
152 250 mm, with the majority falling during the summer monsoon season from June to
153 September.

154 Significant creosotebush encroachment at SNWR is believed to have last occurred
155 in the 1950’s, with high shrub recruitment before and after a multi-year drought that

caused a large loss in grass cover, setting the stage for creosotebush expansion (Moreno-de Las Heras et al., 2015; Moreno-de las Heras et al., 2016). The recruitment events that facilitate creosotebush expansion are thought to be highly episodic (Peters and Yao, 2012). Given that creosotebush seedlings have been shown to establish around the time that late-summer heavy rainfall occurs (Boyd and Brum, 1983; Bowers et al., 2004), higher precipitation rates may be responsible for increased recruitment.

Encroachment re-surveys

We recorded shrub percent cover along two permanent 1000-m transects that spanned the shrub-grass ecotone, from high to low to near-zero shrub density. These surveys were conducted in summer 2001 and again in summer 2013 to document change in creosotebush abundance and spatial extent. At every 10 meters, shrub cover was recorded in nine cover classes (<1%, 1–4%, 5–10%, 10–25%, 25–33%, 33–50%, 50–75%, 75–95%, >95%). For visualization, we show midpoint values of these cover classes at each meter location for both transects and years.

Demographic data

Ecotone transects

Collection of demographic data occurred during early June of every year from 2013-2017. This work was conducted at four sites in the eastern part of SNWR (one site was initiated in 2013 and the other three in 2014), with three transects at each site (different transects than those used for re-surveys). All transects were placed along a shrubland-grassland ecotone so that a full range of shrub densities was captured: each transect spanned core shrub areas, grassland with few shrubs, and the transition between them. Lengths of these transects varied from 200 to 600 m, determined by the strength of vegetation transition since “steep” transitions required less length to capture the full range of shrub densities.

181 We quantified shrub density in 5-meter “windows” along each transect, including all
 182 plants within one meter of the transect on either side. Densities were quantified once for
 183 each transect (in 2013 or 2014) and were assumed to remain effectively constant for the
 184 duration of the study, a reasonable assumption for a species with very low recruitment
 185 and very high survival of established plants. Given the population’s size structure, we
 186 weighted the density of each window by the sizes of the plants, which we quantified as
 187 volume (cm^3). Volume was calculated as that of an elliptic cone: $V_i = \frac{\pi h}{3} \frac{lw}{4}$ where l , w ,
 188 and h are the maximum length, maximum width, and height, respectively. Maximum
 189 length and width were measured so that they were always perpendicular to each other,
 190 and height was measured from the base of the woody stem at the soil surface to the
 191 highest part of the shrub. The weighted density for a window was then expressed as
 192 $\log(\text{volume})$ summed over all plants in the window.

193 **Observational census**

194 At 50-m intervals along each transect we tagged up to 10 plants for annual demographic
 195 census and recorded their local (5-m resolution) window so that we could connect indi-
 196 vidual demographic performance to local weighted density. These tagged shrubs were
 197 revisited every June and censused for survival (alive/dead), size (width, length, and
 198 height, as above), and reproduction (numbers of flowers and fruits). In instances where
 199 shrubs had large numbers of reproductive structures that would be difficult to reliably
 200 count (a large shrub may have many hundreds of flowers or fruits), we made counts on a
 201 fraction of the shrub and extrapolated to estimate whole-plant reproduction. Creosote-
 202 bush does not have a discrete reproductive season, instead producing flowers and fruits
 203 over much of the warm season. Our measurements of reproductive output are therefore
 204 conservative, and likely underestimate cumulative seed production for an entire transi-
 205 tion year. Each year, we also searched for new recruits within one m on either side of
 206 the transect. New recruits were tagged and added to the demographic census.

207 Transplant experiment

208 We conducted a transplant experiment in 2015 to test how shrub density affects seedling
209 survival. This approach complemented observational estimates of density dependence
210 and filled in gaps for a part of the shrub life cycle that is rarely observed due to low re-
211 cruitment. Seeds for the experiment were collected from plants in our study population in
212 2014. Seeds were germinated on Pro-Mix potting soil (Quakertown, PA) in Fall 2014 and
213 seedlings were transferred to 3.8 cm-by-12.7 cm cylindrical containers and maintained in
214 a greenhouse at Rice University. Seedlings were transported to SNWR and transplanted
215 into our experimental design during July 27-31 2015. Transplant timing was intended to
216 coincide with the start of the monsoon season, when most natural recruitment occurs.

217 The transplant experiment was conducted at the same four sites and three transects
218 per site as the observational demographic census, where we knew weight shrub densities
219 at 5-m window resolution. Along each transect we established 12 1-m by 1-m plots.
220 Plots were intentionally placed to capture density variation: four plots were in windows
221 with zero shrubs, four plots were placed in the top four highest-density windows, and
222 the remaining four plots were randomly distributed among the remaining windows with
223 weighted density greater than zero. Plots were placed in the middle of each 5-m window
224 (at meter 2.5). Plots were divided into four 0.5-m by 0.5-m subplots. We divided each
225 subplot into nine squares and recorded ground cover of each square as one of the following
226 categories: bare, creosotebush, black grama (*B. eriopoda*), blue grama (*B. gracilis*),
227 other grass, or “other”. Each subplot received one transplanted subplot, for a total of
228 48 transplants per transect, 144 transplants per site, and 576 transplants in the entire
229 experiment. Each site was set up on a different day and there was a significant monsoon
230 event after the third and before the fourth site. This resulted in differential mortality
231 that appears to be related to site (the soil was moist at the fourth site at the time of
232 transplanting, which favored survival) but more likely reflects the timing of the monsoon
233 event relative to planting. We revisited the transplant experiment on October 24, 2015 to

234 survey mortality. After that first visit, transplants were censused along with the naturally
235 occurring plants each June, following the methods described above.

236 **Demographic analysis**

237 We fit statistical models to the demographic data and used AIC-based model selection to
238 evaluate empirical support for alternative candidate models. The top statistical models
239 were then used as the vital rate sub-models of the SIPM, so there is a strong connection
240 between the statistical and population modeling, as is typical of integral projection mod-
241 eling. Our analyses focused on the following demographic vital rates: survival, growth,
242 probability of flowering, flower and fruit production, and seedling recruitment. All of
243 these except recruitment were modeled as a function of plant size, and all of them in-
244 cluded the possibility of density dependence, since we could connect the demographic
245 performance of individual shrubs to the weighted density of their transect window.

246 The alternative hypotheses of pushed versus pulled wave expansion ultimately rest
247 on how demographic vital rates, and the rate of population increase (λ) derived from
248 the combination of all vital rates, respond to density. We were particularly interested in
249 whether demographic performance was maximized as local density goes to zero (pulled)
250 or at non-zero densities behind the wave front (pushed). To flexibly model density
251 dependence and detect non-monotonic responses, we used generalized additive models in
252 the R package ‘mgcv’ (Wood, 2017). For each vital rate, we fit candidate models with
253 or without a smooth term for local weighted density (among other possible covariates).
254 To avoid over-fitting, we set the ‘gamma’ argument of `gam()` to 1.2, which increases
255 the complexity penalty, results in smoother fits (Wood, 2017), and makes our approach
256 more conservative. We pooled data across transition years for demographic analysis. All
257 models included the random effect of transect; we did not attempt to model both site
258 and transect-within-site random effects due to the low numbers of each. All vital rate
259 functions used the natural logarithm of volume (cm^3) as the size variable and the sum

260 $\log(\text{volume})$ as the weighted density of a transect window.

261 **Survival** We modeled survival or mortality in year $t + 1$ as a Bernoulli random variable
262 with three candidate models for survival probability. These included smooth terms for
263 initial size in year t only (1), initial size and weighted density (3), and both smooth terms
264 plus an interaction between initial size and weighted density. We analyzed survival of
265 experimental transplants and observational census plants together in the same analyses,
266 with a fixed effect of ‘transplant’ included in all candidate models. Since recruits and thus
267 mortality events were both very rare in the observational survey, this approach allowed
268 us to “borrow strength” over both data sets to generate a predictive function for size and
269 possibly density -dependent survival while statistically accounting for differences between
270 experimental and naturally occurring plants. Because we had additional, finer-grained
271 cover data for the transplant experiment that we did not have for the observational cen-
272 sus, we conducted an additional stand-alone analysis of transplant survival that explored
273 the influence of covariates at multiple spatial scales (Appendix).

274 **Growth** We modeled size in year $t + 1$ as a Gaussian random variable. There were
275 nine candidate models for growth (Table). The simplest model (1) defined the mean of
276 size in year $t + 1$ as a smooth function of size in year t and constant variance. Models
277 (2) and (3) had constant variance but the mean included smooth terms for initial size
278 and weighted density (2) or both smooth terms plus an interaction between initial size
279 and weighted density (3). Models 4-6 had the same mean structure as 1-3 but defined
280 the standard deviation of size in year $t + 1$ as a smooth function of initial size. Models
281 7-9 mirrored 4-6 and additionally included a smooth term for weighted density in the
282 standard deviation.

283 **Flowering and fruit production** We modeled shrub reproductive status (vegetative
284 or flowering) in year t as a Bernoulli random variable with three candidate models for

flowering probability. These included smooth terms for current size (in year t) only (1), size and weighted density (3), and both smooth terms plus an interaction between size and weighted density. We modeled the reproductive output of flowering plants (the sum of flowerbuds, open flowers, and fruits) in year t as a negative binomial random variable. There were three candidate models for mean reproductive output that corresponded to the same three candidates for flowering probability.

Recruitment We modeled seedling recruitment in each transect window as a binomial random variable given the number of seeds produced in that window in the preceding year. To estimate window-level seed production, we used the best-fit models for flowering and fruit production and applied this to all plants in each window that we observed in our initial density surveys.

Integral Projection Model

The size- and density-dependent statistical models comprised the sub-models of an Integral Projection Model that we used to evaluate how the shrub population growth rate responded to conspecific density. A basic density-independent IPM predicts the number of individuals of size x' at time $t + 1$ ($n(x', t + 1)$) based on a projection kernel (K) that gives the rates of transition from sizes x to x' and is integrated over the size distribution from the minimum (L) to maximum (U) sizes. As in our statistical modeling, the size variable of the IPM (x, x') was $\log(\text{cm}^3)$. In our model, the projection kernel was additionally dependent on local density, which we represent with \tilde{N} .

$$n(x', t + 1) = \int_L^U K(x', x, \tilde{N}) n(x, t) dx \quad (1)$$

For our model, the demographic transitions captured by the projection kernel include growth or shrinkage (G) from size x to x' , conditioned on survival (S) at size x , and the production of new size- x' individuals from size- x parents. Reproduction reflects the

number of seeds produced at size x (F), conditioned on flowering (P), the per-seed probability of recruitment (R), and the size distribution of recruits (C). Thus, we can express the projection kernel as:

$$K(x', x) = S(x, \tilde{N})G(x', x, \tilde{N}) + P(x, \tilde{N})F(x, \tilde{N})R(\tilde{N})C(x') \quad (2)$$

In the statistical modeling, we explored density (\tilde{N}) effects in all of these vital rates except the recruit size distribution. We observed only XX natural recruits during our study, so we were not able to connect recruit size to local density. Instead, we used the pooled recruits to estimate a mean and standard deviation of recruit size assuming a Gaussian distribution.

For analysis, we evaluated the IPM kernel functions at a range of local densities (\tilde{N}), from the minimum to the maximum of weighted density values from the 5-meter windows. At each density level, we discretized the IPM kernel into XX bins and calculated the asymptotic growth rate $\lambda(\tilde{N})$ as the leading eigenvalue of the approximating matrix. We extended the lower (L) and upper (U) integration limits to avoid unintentional “eviction” using the floor-and-ceiling method (Williams et al., 2012).

We sought to characterize the “shape” of density dependence: whether fitness declined monotonically or not with increasing density. We quantified uncertainty in the density-dependent growth rate $\lambda(\tilde{N})$ by bootstrapping our data. For each bootstrap, we randomly sampled XX% of our demographic data, re-ran the statistical modeling and model selection, and used the top vital rate models to generate $\lambda(\tilde{N})$ for that data subset. We repeated this procedure for 500 bootstrap replicates.

Dispersal modelling

Dispersal kernels were calculated using the WALD, or Wald analytical long-distance dispersal, model that uses a mechanistic approach to predict dispersal patterns of plant

propagules by wind. The WALD model, which is largely based in fluid dynamics, can serve as a good approximation of empirically-determined dispersal kernels (Katul et al., 2005; Skarpaas and Shea, 2007) and may be used when empirical dispersal data is not readily available. Under the assumptions that wind turbulence is low, wind flow is vertically homogenous, and terminal velocity is achieved immediately upon seed release, the WALD model simplifies a Lagrangian stochastic model to create a dispersal kernel that estimates the likelihood a propagule will travel a given distance (Katul et al., 2005). This dispersal kernel takes the form of the inverse Gaussian distribution

$$p(r) = \left(\frac{\lambda'}{2\pi r^3} \right)^{\frac{1}{2}} \exp \left[-\frac{\lambda'(r - \mu')^2}{2\mu'^2 r} \right] \quad (3)$$

that is a slight adaptation from equation 5b in Katul et al. (2005), using r to denote dispersal distance. Here, λ' is the location parameter and μ' is the scale parameter, which depend on environmental and plant-specific properties of the study system. The location and scale parameters are defined as $\lambda' = (H/\sigma)^2$ and $\mu' = HU/F$; these are functions of the height H of seed release, wind speed U at seed release height, seed terminal velocity F , and the turbulent flow parameter σ that depends on both wind speed and local vegetation roughness.

In order to create the dispersal kernel, we first take the wind speeds at measurement height z_m and correct them to find wind speed U for any height H by using the logarithmic wind profile

$$U = \frac{1}{H} \int_{d+z_0}^H \frac{u^*}{K} \log \left(\frac{z-d}{z_0} \right) dz \quad (4)$$

given in Bullock et al. (2012) equation 6, with the notation slightly modified. Here, z is the height above the ground, K is the von Karman constant, and u^* is the friction velocity. The zero-plane displacement d and roughness length z_0 are surface roughness parameters that, for a grass canopy height h above the ground, are approximated by

357 $d \approx 0.7h$ and $z_0 \approx 0.1h$. These estimates are from Raupach (1994) for a canopy area
 358 index $\Lambda = 1$ in which the sum of grass canopy elements is equal to the unit area being
 359 measured. A 0.15 m grass height at the study site gives $d = 0.105$ and z_0 , which are
 360 suitable approximations for grassland (Wiernga, 1993). Calculations of u^* were done
 361 using equation A2 from Skarpaas and Shea (2007), in which

$$362 \quad u^* = KU_m \left[\log \left(\frac{z_m - d}{z_0} \right) \right]^{-1} \quad (5)$$

363 and U_m is the mean wind velocity at the measurement height z_m . Values for the turbulent
 364 flow parameter σ were then calculated using the estimate made by Skarpaas and Shea
 365 (2007) in their equation A4, where

$$366 \quad \sigma = 2A_w^2 \sqrt{\frac{K(z - d)u^*}{C_0U}} \quad (6)$$

367 and C_0 is the Kolmogorov constant. A_w is a constant that relates vertical turbulence
 368 to friction velocity and is approximately equal to 1.3 under the assumptions of above-
 369 canopy flow made by Skarpaas and Shea (2007), based off calculations from Hsieh and
 370 Katul (1997). In addition, the assumption that $z = H$ was made in order to make the
 371 calculation of σ more feasible.

372 The values from the previous three equations give us the necessary information to
 373 calculate μ' and λ' , thus allowing us to create the WALD distribution $p(r)$. However, the
 374 base WALD model does not take into account variation in wind speeds or seed terminal
 375 velocities, which limits its applicability in systems where such variation is present. In
 376 order to account for this variation, we integrate the WALD model over distributions these
 377 two variables using the same method as Skarpaas and Shea (2007). The WALD model
 378 assumes seed release from a single point source, though, which is not realistic for a shrub;
 379 because seeds are released across the entire height of the shrub rather than from a point
 380 source, $p(r)$ was also integrated across the uniform distribution from the grass canopy

height to the shrub height. Thus, under the assumptions that the height at which a seed is located does not affect its probability of being released and that seeds are evenly distributed throughout the shrub, this gives the dispersal kernel $K(r)$, where

$$K(r) = \iiint p(F)p(U)p(z)p(r) dF dU dz \quad (7)$$

and $p(F)$ and $p(U)$ are the PDFs of the terminal velocity F and wind speed U , respectively, and $p(z)$ is the uniform distribution from h to H .

The distribution $p(F)$ in the integral above was constructed using experimentally determined seed terminal velocities. This was done by using a high-speed camera and motion tracking software to determine position as a function of time, and then using the Levenberg-Marquardt algorithm to solve a quadratic-drag equation of motion for F . Before seeds were released, they were dried and then dyed with yellow fluorescent powder, and then put against a black background to improve visibility and make tracking easier. While the powder added mass to the seeds, this added mass only yielded an approximately 2.5% increase and was thus negligible, likely having little effect on their terminal velocities. Measurements were conducted for 48 seeds that were randomly chosen from a seed pool derived from different plants, and then an empirical PDF of terminal velocities was constructed using the data. Constructing $p(U)$ involved creating an empirical PDF of hourly wind speeds at Five Points, the site closest to the 12 transects being used, that were obtained from meteorological data collected at the Sevilleta National Wildlife Refuge from 1988 to 2010. We did not weight $p(U)$ and assumed that the probability seed release from the shrub is the same regardless of wind speed.

Spatial integral projection model

Given that the shrub population at this site is approximately homogeneous perpendicular to the direction of encroachment, expansion is modelled as a wave moving in one

dimension. A spatial integral projection model (SIPM) is used to estimate the speed at which encroachment occurs; such a model incorporates the effects of variation in traits like plant size that stage-structured models, such as those described in Neubert and Caswell (2000), do not capture. According to Jongejans et al. (2011), a general SIPM can be formulated as

$$\mathbf{n}(x_2, z_2, t + 1) = \iint \tilde{K}(x_2, x_1, z_2, z_1) \mathbf{n}(x_1, z_1, t) dx_1 dz_1 \quad (8)$$

where x_1 and x_2 are locations of individuals of a particular size before and after one unit of time, and z_1 and z_2 are the respective sizes. The vector \mathbf{n} indicates the population density of each size, and \tilde{K} is a kernel that combines dispersal with demography. Though this SIPM represents a continuous spectrum of shrub sizes and densities, it was implemented by discretising the above integral with a 200 x 200 matrix, as this makes calculations significantly more tractable.

Movement of the wave is determined by the components of the combined dispersal/demography kernel \tilde{K} , which is of the same form as that used in Jongejans et al. (2011). Here,

$$\tilde{K}(x_2, x_1, z_2, z_1) = K(x_2 - x_1)Q(z_2 - z_1) + \delta(x_2 - x_1)G(z_2 - z_1) \quad (9)$$

and K is the dispersal kernel, Q a reproduction function, G a growth function, and δ the Dirac delta function. G is derived from the model for annual growth ratio, and Q is derived from the reproductive structures model as well as other factors including number of seeds per reproductive structure, probability of recruitment from seed, and recruit size. Both G and Q give the probability of transition between sizes; in the case of G , this is the probability of growing from one specific size to another, and in the case of Q the probability that an individual of a specific size produces a recruit of a specific size. The product of K and Q represents the production and dispersal of motile propagules, while

the product of G and δ represents the growth of sessile individuals.

Given growth function G and the reproduction function Q , the speed of the moving wave can be calculated as

$$c^* = \min_{s>0} \left[\frac{1}{s} \ln(\rho_s) \right] \quad (10)$$

where s is the wave shape parameter and ρ_s is the dominant eigenvalue of the kernel \mathbf{H}_s (Jongejans et al., 2011). This estimate for the wavespeed is valid under the assumption that population growth decreases monotonically as conspecific density increases, with the highest rates of growth occurring at the lowest population densities (Lewis et al., 2006). The kernel \mathbf{H}_s is defined as

$$\mathbf{H}_s = M(s)Q(z_2 - z_1) + G(z_2 - z_1) \quad (11)$$

where $M(s)$ is the moment-generating function of the dispersal kernel (Jongejans et al., 2011). For one-dimensional dispersal, this moment-generating function can be estimated as

$$M(s) = \frac{1}{N} \sum_{i=1}^n I_0(sr_i) \quad (12)$$

where r is the dispersal distance for each observation, and I_0 is the modified Bessel function of the first kind and zeroth order (Skarpaas and Shea, 2007). In order to obtain M , numerous dispersal distances were simulated from the dispersal kernel $K(r)$ described in the previous section, with over 2000 replications for each shrub height increment of 1 cm. This was performed over the range from the lowest possible dispersal height to the maximum shrub height. Once $M(s)$ was obtained for dispersal at each shrub height, \mathbf{H}_s and c^* were calculated for each value of s ; this was done for values of s ranging from 0 to 2, as it is this range in which c^* occurs.

Estimates of the wavespeed were bootstrapped for a total of 1000 replicates. Each bootstrap replicate recreated size- and density-dependent demographic models using 80%

453 resampling on the original demographic data, and recreated dispersal kernels also using
 454 80% resampling on the wind speeds and seed terminal velocities. Between replicates,
 455 the structure of the demographic models was kept constant, though coefficient estimates
 456 were not; this approach, while effectively ignoring model uncertainty, has the benefit of
 457 increasing computational efficiency, which is especially useful given the time-consuming
 458 nature of numerically estimating the many dispersal kernels used in the model.

459 Results

460 Encroachment re-surveys

461 Figure 2.

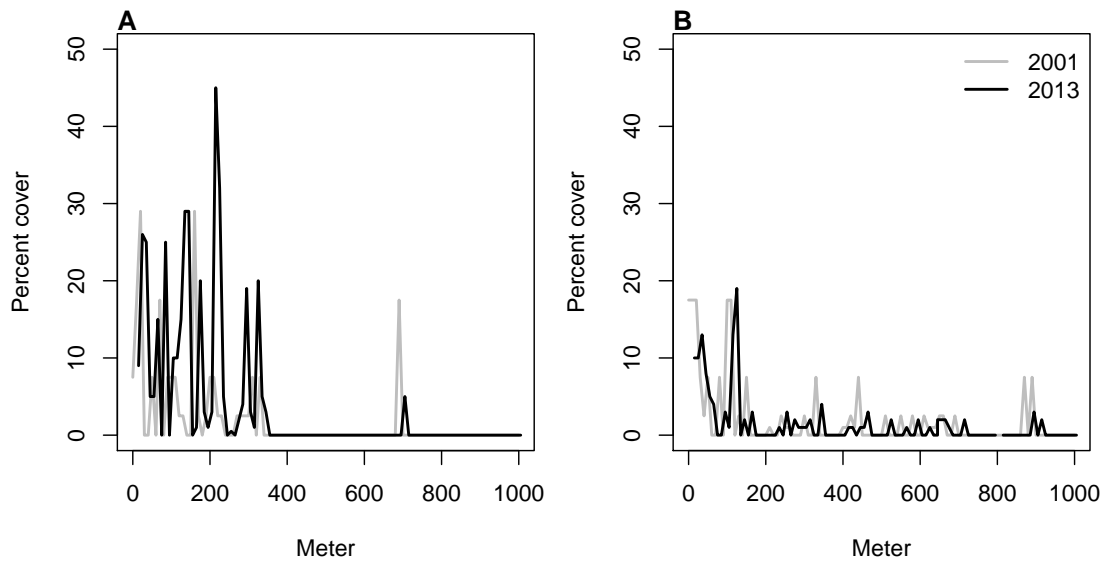


Figure 2: Re-surveys of shrub cover along two permanent trasects (A,B) surveyed in 2001 and 2013.

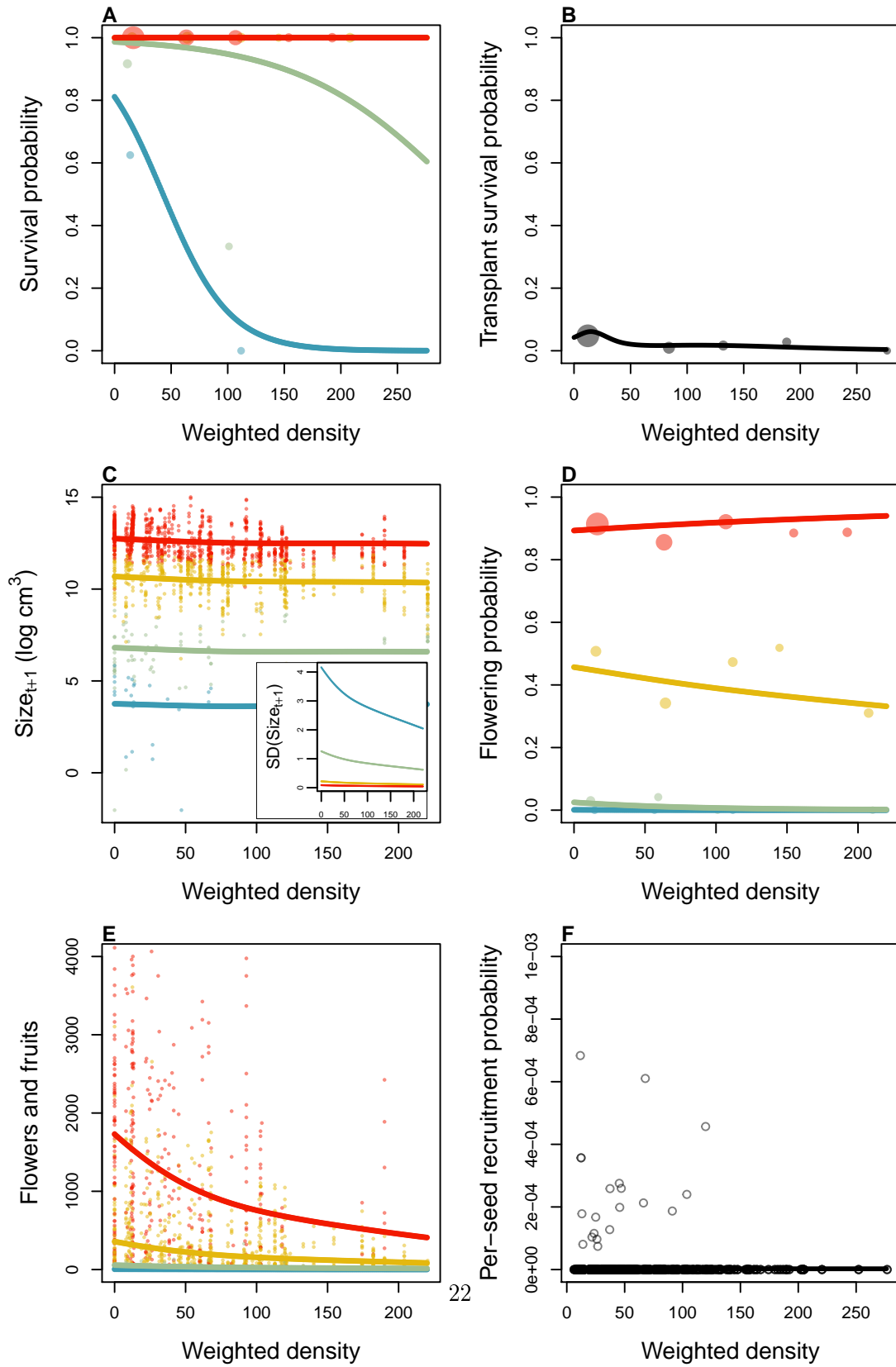


Figure 3: Size- and density-dependence in demographic vital rates.

463 **Survival**

464 **Growth**

465 **Flowering and fruit production**

466 **Recruitment**

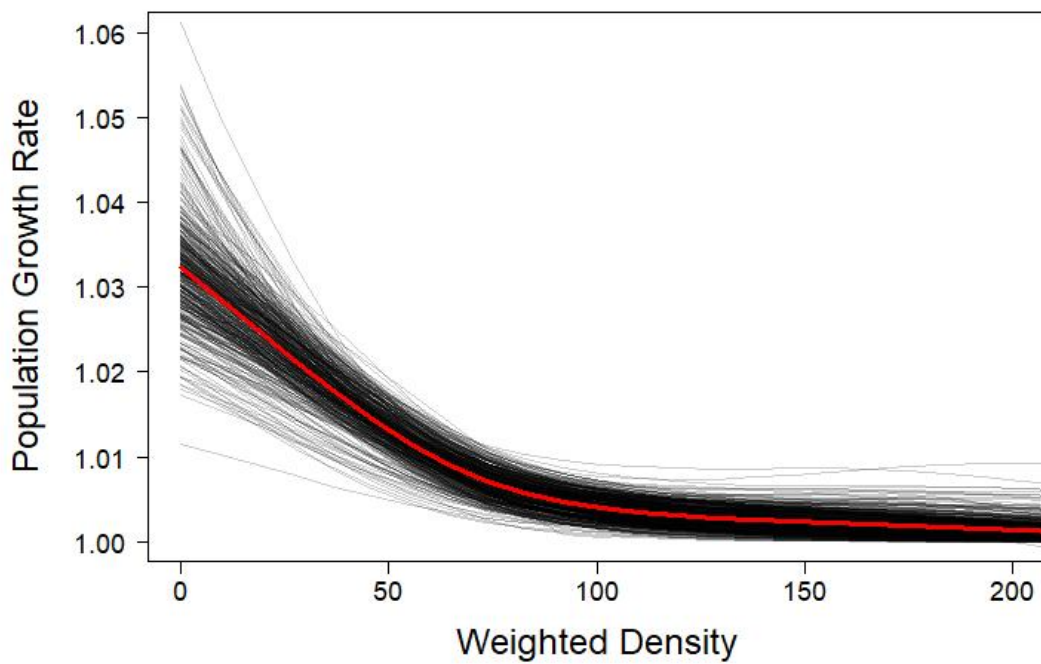


Figure 4: Density dependence in the geographic population growth rate (λ).

467 **Population growth rate** The speed of encroachment at the study site as estimated
468 by the SIPM is rather slow; as can be seen in Figure 5, the low-density wavefront moves
469 at approximately 0.5 cm/yr under normal conditions and at 1 cm/yr under the best
470 seedling survival conditions observed in the dataset. These improved conditions were
471 observed due to above-average rainfall that occurred after greenhouse-grown seedlings

472 were transplanted to the site. Population growth in this low-density region of the mov-
 473 ing wave is also low, with a geometric growth rate of $\lambda \approx 1.006$ and even lower rates of
 474 growth the higher-density regions behind; in the higher-survival scenario the maximum
 475 rate increases to $\lambda \approx 1.013$, with growth still decreasing as density increases. For both
 476 scenarios, the decrease in population growth rate with increasing density was monotonic
 477 across the range of observed standardised densities, as is shown in Figure 5. This suggests
 478 that an Allee effect is likely not present in this population, as the highest rate of popula-
 479 tion growth is found at the lowest density vanguard of the encroaching population. Thus,
 480 the conditions necessary for equation 9 to be valid are satisfied, and these wavespeeds
 481 are applicable for a pulled-wave scenario in which no Allee effects are present.

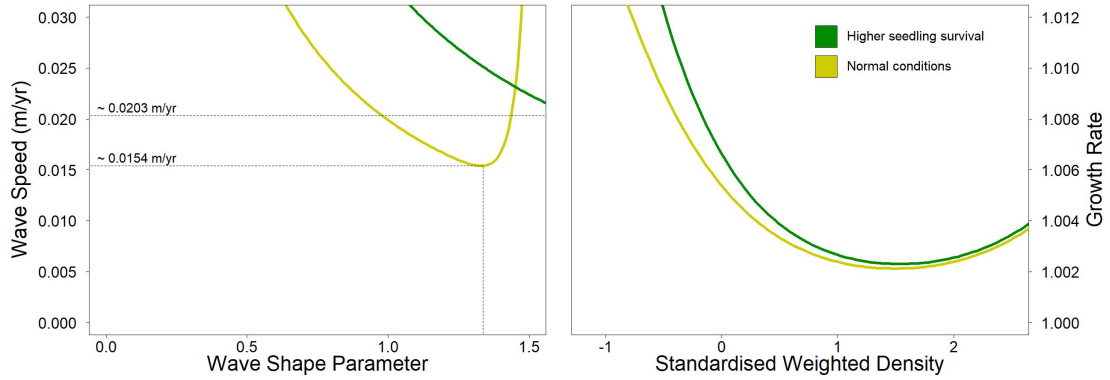


Figure 5: Estimated encroachment wave speeds (left) and geometric rates of population growth (right) for higher post-rainfall seedling survival and normal conditions.

482 As the speed of encroachment is quite limited, so is the extent of wind dispersal.
 483 Long distance dispersal events, while more common for taller shrubs than their shorter
 484 counterparts, are still uncommon overall. For the tallest shrub height of 1.98 m, only
 485 0.32% of propagules exceed a dispersal distance of 5 m, and 0.02% exceed 10 m. At 1
 486 m, or approximately half the tallest shrub height, long distance dispersal is even less
 487 likely, with 0.0046% of propagules exceeding a dispersal distance of 5 m and 0.0009%
 488 exceeding 10 m. Given that the median shrub height is only 0.64 m, the occurrence of

489 long-distance wind dispersal in most of the shrub population is highly improbable, and
490 the few instances in which it occurs will only be limited to the tallest shrubs. Thus, as
491 Figure 6 demonstrates, shorter dispersal distances dominate; even for the tallest shrub,
492 81% of seeds fall within only a metre of the plant, and this percentage increases as
493 shrub height decreases. Dispersal kernels have their highest probability density at dis-
494 persal distances between 2 and 8 cm from the shrub; here, as shrub height increases, the
495 most probable dispersal distance slightly increases while maximum probability density
496 decreases. Regardless of the shrub height, most dispersal will occur very close to the
497 plant, though increases in shrub height dramatically increase the likelihood of dispersal
498 at longer distances. It is clear that the shape of the height-dependent dispersal kernel
499 $K(r)$ varies greatly among the shrub population given the large range of shrub heights
500 observed; shrubs at lower heights have more slender kernels with most of the seeds dis-
501 persing closer to the plant, while taller shrubs have kernels with much fatter tails and
502 are more capable of longer-distance dispersal.

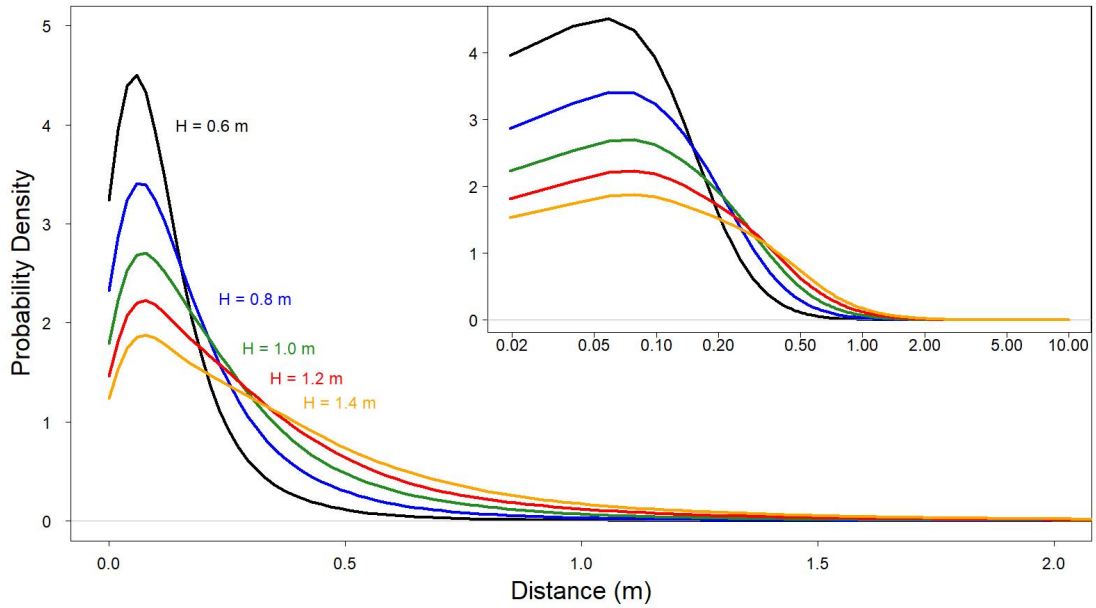


Figure 6: Dispersal kernels, with each colour representing a selected shrub height. The inset plot is the same as the large plot, though with a logarithmic x-axis to more easily show differences in dispersal probability at smaller distances.

503 Density and size dependence are evident in all 4 of the demographic rates, with
 504 coefficients for each model displayed in Table 2. For growth, reproduction, and survival,
 505 density dependence is mostly negative and monotonic; this is not the case for probability
 506 of flowering, where shrub size seems to be more important than the effects of density alone
 507 and suggests that larger shrubs have a higher probability of flowering than their smaller
 508 counterparts. This, along with size and density dependence in growth and reproduction,
 509 is shown in Figure 7. Size dependence is positive for reproduction, as would be expected
 510 since larger plants typically produce more flowers and fruits. However, annual growth
 511 decreases as size increases; this could be in part due to the annual growth in this study
 512 being quantified as a proportion relative to the shrub's initial size. While larger shrubs
 513 may produce more plant material over a year in terms of absolute volume, smaller shrubs
 514 produce less but can still have higher annual growth in terms of the percentage of volume

515 added relative to their initial volume. When compared to density, shrub size is a much
516 stronger predictor of survival, with significant differences in mortality rates depending on
517 shrub size. For small shrubs, mortality is exceptionally high, and increases in volume for
518 these shrubs only slightly increase the likelihood of survival. However, after shrubs reach
519 a logarithmic volume of approximately 7.3, they are almost guaranteed to survive, with
520 survival rates near 100% persisting regardless of any further size increases. Interestingly,
521 though most recruits were found at lower densities, the probability of recruitment from
522 seed displays positive density dependence; the probability of recruitment was still very
523 low, though, with a baseline rate of approximately 2 recruits per 10,000 seeds.

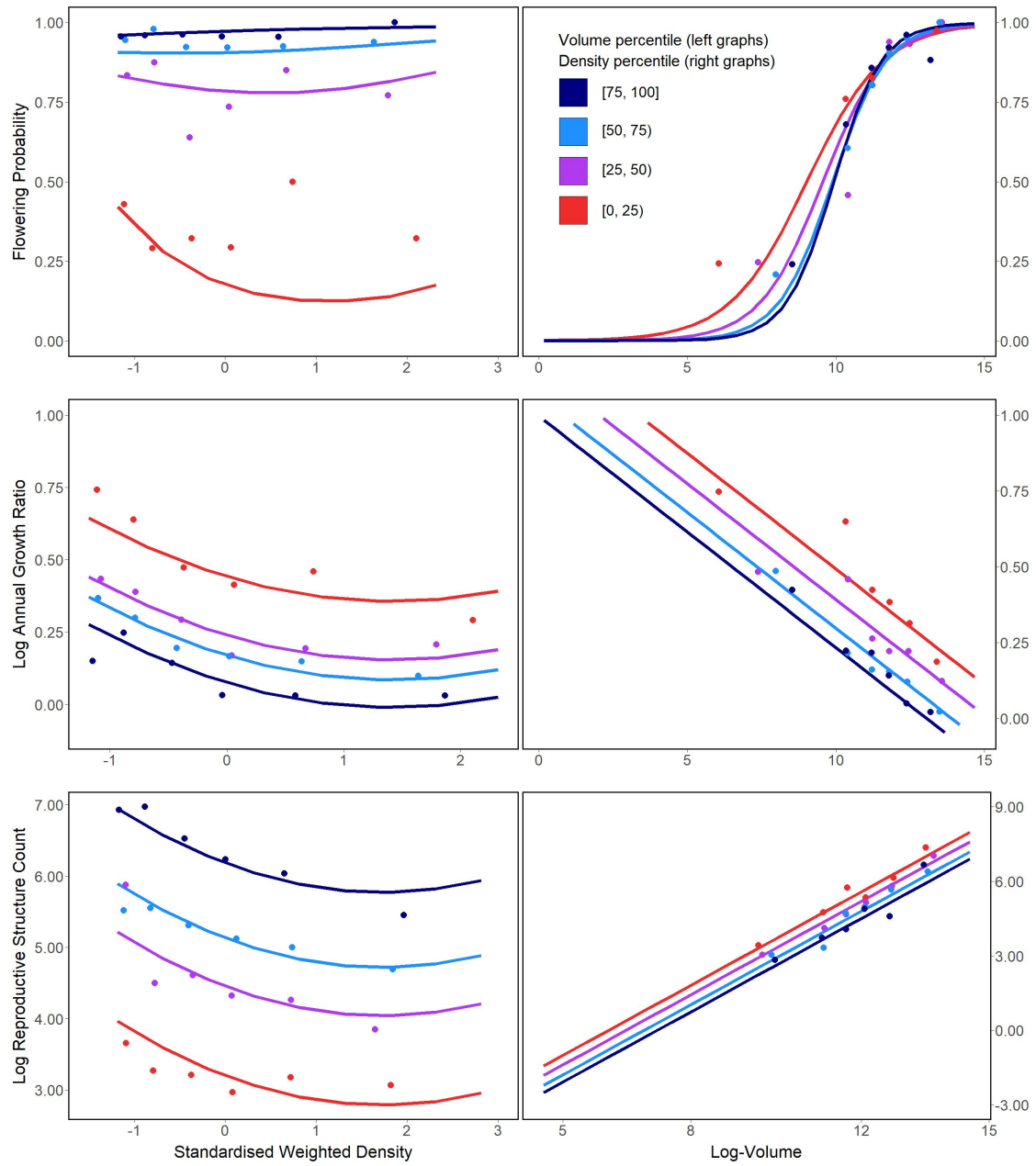


Figure 7: Flowering probability (top row), log annual growth ratio (centre row), and log reproductive structure count (bottom row) at all four sampling sites. In the left column of graphs, the three response variables are shown as a function of density for each of four volume quartiles, with each quartile containing six density bins; in the right column, the opposite occurs, with response variables shown as functions of four volume quartiles that each contain six density bins. Graphs quantifying the number of reproductive structures include data only on plants that flowered.

Discussion

The slow movement of the encroaching creosotebush wave at the Sevilleta LTER site can likely be contributed to a combination of three factors: short dispersal distances with extremely limited long-distance dispersal events, very low probability of recruitment from seed, and high seedling mortality. These three barriers, when combined, form a formidable challenge to the establishment of new shrubs at the low-density front of the wave. First, a seed must travel far enough to avoid competition with the parent shrub, which is unlikely given the dispersal kernels shown in Figure 2. Even if the seed manages to be dispersed this far, its chances of becoming a seedling are low. Caching and consumption by seed-eaters such as a variety of seed-harvesting ants (Whitford, 1978; Whitford et al., 1980; Lei, 1999) and the kangaroo rat *Dipodomys merriami* (Chew and Chew, 1970) decreases the amount of seeds available for germination. However, reduction in germination caused by destruction of seeds may be partly mitigated by the more favourable germination conditions that these seeds can experience when cached underground (Chew and Chew, 1970). Many of the remaining seeds will still fail to germinate, and in the unlikely event that germination does occur, seedlings will likely die given the high rates of mortality observed in smaller shrubs. Such high rates of creosotebush seedling mortality have been observed in other studies as well (Boyd and Brum, 1983; Bowers et al., 2004), probably due to a combination of herbivory, competition, and abiotic stresses.

However, as low as they are, the wavespeed estimates given in this paper are still conservative estimates for reasons mostly related to dispersal. First, it is important to note that the dispersal kernels used here, while they account for variation in factors such as wind speed and terminal velocity, may underestimate the distances that shrub propagules travel. Because the WALD model assumes that terminal velocity is reached immediately upon seed release, seeds in the estimate thus take a shorter time to fall

550 and have less time to be transported by wind, and the true frequency of long-distance
551 dispersal events may thus be greater than what is estimated here. Second, dispersal at the
552 study site could occur through additional mechanisms other than wind. For example,
553 secondary dispersal through runoff from significant rainfall events can transport seeds
554 (Thompson et al., 2014), and given that long-distance dispersal by bird and subsequent
555 species divergence is thought to be responsible for creosotebush being in North America
556 in the first place (Wells and Hunziker, 1976), short-distance dispersal by other animals
557 at the study site likely occurs. As mentioned above, seeds are transported by seed-
558 harvesting ants and granivorous mammals, where they are often stored in caches that
559 can be appreciable distances from the parent shrubs. Whether transportation occurs via
560 ant or rodent, creosotebush seeds can be moved significantly further than wind alone
561 can, though many of these seeds are eventually consumed.

562 Despite the more conservative estimates our model yields, the estimated rate of dis-
563 persal in creosotebush populations at the Sevilleta National Wildlife Refuge is consistent
564 with observations from the past 50-60 years, as creosotebush expansion during this time
565 has been minimal (Moreno-de las Heras et al., 2016). However, it cannot explain the
566 long-term increases in creosotebush cover at the study site, as total encroachment over
567 the past 150 years is much greater than what would be expected given the encroachment
568 rates derived by our models. Such a discrepancy is likely due to much of the expansion
569 occurring in an episodic fashion, with short times during which rapid encroachment oc-
570 curs due to favourable environmental conditions. This could be due in part to seedling
571 recruitment, which is a factor that strongly limits creosotebush expansion, being rare
572 and episodic. For example, Allen et al. (2008) estimate that a major recruitment event
573 occurred at this site in the 1950s, which is supported by photographic evidence from
574 Milne et al. (2003) of a drought-driven expansion during this time. Moreno-de las Heras
575 et al. (2016) estimate that after this expansion, several smaller creosotebush recruitment
576 events occurred in decadal episodes. However, such events can be highly localised and

577 may not necessarily occur at the low-density front of encroachment, which could explain
578 how these recruitment events can still coexist with lack of encroachment in the recent
579 past.

580 Overall, our observations and model highlight three aspects of creosotebush encroach-
581 ment that should be the focus of future studies seeking to obtain better estimates of
582 encroachment rates. First, negative density dependence in survival, growth, and repro-
583 duction is demonstrated, along with size dependence. The clear dependence on size and
584 conspecific density suggests that they both should be considered when estimating cre-
585 osotebush expansion and quantifying the demographic variation that contributes to it.
586 Second, wind dispersal in these shrubs is quite limited; though the dispersal kernels seen
587 here are typical in the sense that they are characterised by high near-plant dispersal and
588 exceptionally low long-distance dispersal, the scale across which such dispersal occurs
589 is small, with most seeds landing within only 1 m of the shrub. Wind dispersal alone
590 may be an underestimate of the true amount of dispersal occurring, and future work
591 should seek to incorporate the effects of dispersal by runoff and animals so that a more
592 representative model of total dispersal can be obtained. Finally, encroachment is slow or
593 even stagnates, but only most of the time. Though our encroachment speed estimates
594 are representative of creosotebush populations for most years, the significant expansion
595 seen over larger time scales suggests that there is episodic expansion in other years; while
596 our model is consistent with the recent stagnation in creosotebush encroachment at the
597 Sevilleta LTER site, a model that also includes interannual variability in factors such
598 as survival and recruitment would be able to better account for instances of episodic
599 population expansion that are characteristic of this location.

600 Acknowledgements

601 Author contributions

602 Data accessibility

603 References

- 604 Allen, A., W. Pockman, C. Restrepo, and B. Milne. 2008. Allometry, growth and
605 population regulation of the desert shrub *Larrea tridentata*. *Functional Ecology* pages
606 197–204.
- 607 Bowers, J. E., R. M. Turner, and T. L. Burgess. 2004. Temporal and spatial patterns in
608 emergence and early survival of perennial plants in the Sonoran Desert. *Plant Ecology*
609 **172**:107–119.
- 610 Boyd, R. S., and G. D. Brum. 1983. Postdispersal reproductive biology of a Mojave Desert
611 population of *Larrea tridentata* (Zygophyllaceae). *American Midland Naturalist* pages
612 25–36.
- 613 Brandt, J. S., M. A. Haynes, T. Kuemmerle, D. M. Waller, and V. C. Radeloff. 2013.
614 Regime shift on the roof of the world: Alpine meadows converting to shrublands in
615 the southern Himalayas. *Biological Conservation* **158**:116–127.
- 616 Buffington, L. C., and C. H. Herbel. 1965. Vegetational changes on a semidesert grassland
617 range from 1858 to 1963. *Ecological monographs* **35**:139–164.
- 618 Bullock, J. M., S. M. White, C. Prudhomme, C. Tansey, R. Perea, and D. A. Hooftman.
619 2012. Modelling spread of British wind-dispersed plants under future wind speeds in
620 a changing climate. *Journal of Ecology* **100**:104–115.

621 Cabral, A., J. De Miguel, A. Rescia, M. Schmitz, and F. Pineda. 2003. Shrub encroach-
622 ment in Argentinean savannas. *Journal of Vegetation Science* **14**:145–152.

623 Chew, R. M., and A. E. Chew. 1970. Energy relationships of the mammals of a desert
624 shrub (*Larrea tridentata*) community. *Ecological Monographs* pages 2–21.

625 D’Odorico, P., J. D. Fuentes, W. T. Pockman, S. L. Collins, Y. He, J. S. Medeiros,
626 S. DeWekker, and M. E. Litvak. 2010. Positive feedback between microclimate and
627 shrub encroachment in the northern Chihuahuan desert. *Ecosphere* **1**:1–11.

628 D’Odorico, P., G. S. Okin, and B. T. Bestelmeyer. 2012. A synthetic review of feedbacks
629 and drivers of shrub encroachment in arid grasslands. *Ecohydrology* **5**:520–530.

630 Gandhi, S. R., E. A. Yurtsev, K. S. Korolev, and J. Gore. 2016. Range expansions
631 transition from pulled to pushed waves as growth becomes more cooperative in an
632 experimental microbial population. *Proceedings of the National Academy of Sciences*
633 **113**:6922–6927.

634 Gardner, J. L. 1951. Vegetation of the creosotebush area of the Rio Grande Valley in
635 New Mexico. *Ecological Monographs* **21**:379–403.

636 Gibbens, R., R. McNeely, K. Havstad, R. Beck, and B. Nolen. 2005. Vegetation changes
637 in the Jornada Basin from 1858 to 1998. *Journal of Arid Environments* **61**:651–668.

638 Goslee, S., K. Havstad, D. Peters, A. Rango, and W. Schlesinger. 2003. High-resolution
639 images reveal rate and pattern of shrub encroachment over six decades in New Mexico,
640 USA. *Journal of Arid Environments* **54**:755–767.

641 Grover, H. D., and H. B. Musick. 1990. Shrubland encroachment in southern New Mexico,
642 USA: an analysis of desertification processes in the American Southwest. *Climatic*
643 *change* **17**:305–330.

- 644 Hsieh, C.-I., and G. G. Katul. 1997. Dissipation methods, Taylor’s hypothesis, and
645 stability correction functions in the atmospheric surface layer. *Journal of Geophysical*
646 *Research: Atmospheres* **102**:16391–16405.
- 647 Huang, H., L. D. Anderegg, T. E. Dawson, S. Mote, and P. D’Odorico. 2020. Crit-
648 ical transition to woody plant dominance through microclimate feedbacks in North
649 American coastal ecosystems. *Ecology* **101**:e03107.
- 650 Jongejans, E., K. Shea, O. Skarpaas, D. Kelly, and S. P. Ellner. 2011. Importance of
651 individual and environmental variation for invasive species spread: a spatial integral
652 projection model. *Ecology* **92**:86–97.
- 653 Katul, G., A. Porporato, R. Nathan, M. Siqueira, M. Soons, D. Poggi, H. Horn, and
654 S. A. Levin. 2005. Mechanistic analytical models for long-distance seed dispersal by
655 wind. *The American Naturalist* **166**:368–381.
- 656 Keitt, T. H., M. A. Lewis, and R. D. Holt. 2001. Allee effects, invasion pinning, and
657 species’ borders. *The American Naturalist* **157**:203–216.
- 658 Kelleway, J. J., K. Cavanaugh, K. Rogers, I. C. Feller, E. Ens, C. Doughty, and N. Sain-
659 tilan. 2017. Review of the ecosystem service implications of mangrove encroachment
660 into salt marshes. *Global Change Biology* **23**:3967–3983.
- 661 Knapp, A. K., J. M. Briggs, S. L. Collins, S. R. Archer, M. S. BRET-HARTE, B. E.
662 Ewers, D. P. Peters, D. R. Young, G. R. Shaver, E. Pendall, et al. 2008. Shrub
663 encroachment in North American grasslands: shifts in growth form dominance rapidly
664 alters control of ecosystem carbon inputs. *Global Change Biology* **14**:615–623.
- 665 Kot, M., M. A. Lewis, and P. van den Driessche. 1996. Dispersal data and the spread of
666 invading organisms. *Ecology* **77**:2027–2042.

- 667 Lei, S. A. 1999. Ecological impacts of *Pogonomyrmex* on woody vegetation of a *Larrea*-
668 *Ambrosia* shrubland. *The Great Basin Naturalist* pages 281–284.
- 669 Lewis, M., and P. Kareiva. 1993. Allee dynamics and the spread of invading organisms.
670 *Theoretical Population Biology* **43**:141–158.
- 671 Lewis, M. A., M. G. Neubert, H. Caswell, J. S. Clark, and K. Shea, 2006. A guide
672 to calculating discrete-time invasion rates from data. Pages 169–192 *in* *Conceptual*
673 *ecology and invasion biology: reciprocal approaches to nature*. Springer.
- 674 Mabry, T. J., J. H. Hunziker, D. Difeo Jr, et al. 1978. Creosote bush: biology and
675 chemistry of *Larrea* in New World deserts. Dowden, Hutchinson & Ross, Inc.
- 676 Maddox, J. C., and S. Carlquist. 1985. Wind dispersal in Californian desert plants:
677 experimental studies and conceptual considerations. *Aliso: A Journal of Systematic*
678 *and Evolutionary Botany* **11**:77–96.
- 679 Milne, B. T., D. I. Moore, J. L. Betancourt, J. A. Parks, T. W. Swetnam, R. R. Par-
680 menter, and W. T. Pockman. 2003. Multidecadal drought cycles in south-central New
681 Mexico: Patterns and consequences. Oxford University Press: New York, NY.
- 682 Moreno-de Las Heras, M., R. Díaz-Sierra, L. Turnbull, and J. Wainwright. 2015. Assess-
683 ing vegetation structure and ANPP dynamics in a grassland–shrubland Chihuahuan
684 ecotone using NDVI–rainfall relationships. *Biogeosciences* **12**:2907–2925.
- 685 Moreno-de las Heras, M., L. Turnbull, and J. Wainwright. 2016. Seed-bank structure
686 and plant-recruitment conditions regulate the dynamics of a grassland-shrubland Chi-
687 huahuan ecotone. *Ecology* **97**:2303–2318.
- 688 Mugasi, S., E. Sabiiti, and B. Tayebwa. 2000. The economic implications of bush
689 encroachment on livestock farming in rangelands of Uganda. *African Journal of Range*
690 *and Forage Science* **17**:64–69.

- 691 Nathan, R., G. G. Katul, G. Bohrer, A. Kuparinen, M. B. Soons, S. E. Thompson,
692 A. Trakhtenbrot, and H. S. Horn. 2011. Mechanistic models of seed dispersal by wind.
693 *Theoretical Ecology* **4**:113–132.
- 694 Neubert, M. G., and H. Caswell. 2000. Demography and dispersal: calculation and
695 sensitivity analysis of invasion speed for structured populations. *Ecology* **81**:1613–
696 1628.
- 697 Oba, G., E. Post, P. Syvertsen, and N. Stenseth. 2000. Bush cover and range condition
698 assessments in relation to landscape and grazing in southern Ethiopia. *Landscape*
699 *ecology* **15**:535–546.
- 700 Pan, S., and G. Lin. 2012. Invasion traveling wave solutions of a competitive system
701 with dispersal. *Boundary Value Problems* **2012**:120.
- 702 Parizek, B., C. M. Rostagno, and R. Sottini. 2002. Soil erosion as affected by shrub
703 encroachment in northeastern Patagonia. *Rangeland Ecology & Management/Journal*
704 *of Range Management Archives* **55**:43–48.
- 705 Peters, D. P., and J. Yao. 2012. Long-term experimental loss of foundation species:
706 consequences for dynamics at ecotones across heterogeneous landscapes. *Ecosphere*
707 **3**:1–23.
- 708 Ratajczak, Z., J. B. Nippert, and S. L. Collins. 2012. Woody encroachment decreases
709 diversity across North American grasslands and savannas. *Ecology* **93**:697–703.
- 710 Raupach, M. 1994. Simplified expressions for vegetation roughness length and zero-
711 plane displacement as functions of canopy height and area index. *Boundary-Layer*
712 *Meteorology* **71**:211–216.
- 713 Ravi, S., P. D’Odorico, S. L. Collins, and T. E. Huxman. 2009. Can biological invasions
714 induce desertification? *The New Phytologist* **181**:512–515.

- 715 Reed, M., L. Stringer, A. Dougill, J. Perkins, J. Atlhopheng, K. Mulale, and N. Favretto.
716 2015. Reorienting land degradation towards sustainable land management: Linking
717 sustainable livelihoods with ecosystem services in rangeland systems. *Journal of envi-*
718 *ronmental management* **151**:472–485.
- 719 Reynolds, J. F., R. A. Virginia, P. R. Kemp, A. G. De Soyza, and D. C. Tremmel. 1999.
720 Impact of drought on desert shrubs: effects of seasonality and degree of resource island
721 development. *Ecological Monographs* **69**:69–106.
- 722 Roques, K., T. O’connor, and A. R. Watkinson. 2001. Dynamics of shrub encroach-
723 ment in an African savanna: relative influences of fire, herbivory, rainfall and density
724 dependence. *Journal of Applied Ecology* **38**:268–280.
- 725 Schlesinger, W. H., and A. M. Pilmanis. 1998. Plant-soil interactions in deserts. *Biogeo-*
726 *chemistry* **42**:169–187.
- 727 Schlesinger, W. H., J. A. Raikes, A. E. Hartley, and A. F. Cross. 1996. On the spatial
728 pattern of soil nutrients in desert ecosystems: ecological archives E077-002. *Ecology*
729 **77**:364–374.
- 730 Schlesinger, W. H., J. F. Reynolds, G. L. Cunningham, L. F. Huenneke, W. M. Jarrell,
731 R. A. Virginia, and W. G. Whitford. 1990. Biological feedbacks in global desertification.
732 *Science* **247**:1043–1048.
- 733 Sirami, C., and A. Monadjem. 2012. Changes in bird communities in Swaziland savannas
734 between 1998 and 2008 owing to shrub encroachment. *Diversity and Distributions*
735 **18**:390–400.
- 736 Skarpaas, O., and K. Shea. 2007. Dispersal patterns, dispersal mechanisms, and invasion
737 wave speeds for invasive thistles. *The American Naturalist* **170**:421–430.

738 Sullivan, L. L., B. Li, T. E. Miller, M. G. Neubert, and A. K. Shaw. 2017. Density depen-
739 dence in demography and dispersal generates fluctuating invasion speeds. *Proceedings*
740 of the National Academy of Sciences **114**:5053–5058.

741 Taylor, C. M., and A. Hastings. 2005. Allee effects in biological invasions. *Ecology*
742 Letters **8**:895–908.

743 Thompson, S. E., S. Assouline, L. Chen, A. Trahktenbrot, T. Svoray, and G. G. Katul.
744 2014. Secondary dispersal driven by overland flow in drylands: Review and mechanistic
745 model development. *Movement ecology* **2**:7.

746 Trollope, W., F. Hobson, J. Danckwerts, and J. Van Niekerk. 1989. Encroachment and
747 control of undesirable plants. *Veld management in the Eastern Cape* pages 73–89.

748 Turnbull, L., J. Wainwright, and R. E. Brazier. 2010. Changes in hydrology and erosion
749 over a transition from grassland to shrubland. *Hydrological Processes: An Interna-*
750 *tional Journal* **24**:393–414.

751 Van Auken, O. 2009. Causes and consequences of woody plant encroachment into western
752 North American grasslands. *Journal of environmental management* **90**:2931–2942.

753 Van Auken, O. W. 2000. Shrub invasions of North American semiarid grasslands. *Annual*
754 *review of ecology and systematics* **31**:197–215.

755 Vasek, F. C. 1980. Creosote bush: Long-lived clones in the Mojave Desert. *American*
756 *Journal of Botany* **67**:246–255.

757 Veit, R. R., and M. A. Lewis. 1996. Dispersal, population growth, and the Allee ef-
758 fect: dynamics of the house finch invasion of eastern North America. *The American*
759 *Naturalist* **148**:255–274.

760 Wang, M.-H., M. Kot, and M. G. Neubert. 2002. Integrodifference equations, Allee
761 effects, and invasions. *Journal of mathematical biology* **44**:150–168.

- 762 Wells, P. V., and J. H. Hunziker. 1976. Origin of the creosote bush (*Larrea*) deserts of
763 southwestern North America. *Annals of the Missouri Botanical Garden* pages 843–861.
- 764 Whitford, W., E. Depree, and P. Johnson. 1980. Foraging ecology of two chihuahuan
765 desert ant species: *Novomessor cockerelli* and *Novomessor albigasterus*. *Insectes Sociaux*
766 **27**:148–156.
- 767 Whitford, W. G. 1978. Structure and seasonal activity of Chihuahua desert ant commu-
768 nities. *Insectes Sociaux* **25**:79–88.
- 769 Wiernga, J. 1993. Representative roughness parameters for homogeneous terrain.
770 *Boundary-Layer Meteorology* **63**:323–363.
- 771 Williams, J. L., T. E. Miller, and S. P. Ellner. 2012. Avoiding unintentional eviction
772 from integral projection models. *Ecology* **93**:2008–2014.
- 773 Wood, S. 2017. *Generalized Additive Models: An Introduction with R*. 2 edition.
774 Chapman and Hall/CRC.